MNRAS **000**, 1–7 (2017) Preprint 4 August 2017 Compiled using MNRAS LATEX style file v3.0

Calibration and Imaging of NGC 1614 ALMA Band 3 Data

Ziad Modak*
Argelander-Institut für Astronomie, Auf dem Hügel 71, D-53121, Bonn, Germany

4 August 2017

ABSTRACT
In the following work, the steps followed for calibration and imaging of NGC 1614, a nearby Luminous infrared Galaxy, are reported. The raw archival data of CO (1–0) transition line observed using the Atacama Large Millimeter/submillimeter Array were calibrated and imaged using the Common Astronomy Software Applications package. The final line emission data cube had a noise level of 5.363 mJy/beam, a restoring beam size of 0.81"×0.50" and a velocity resolution of 2.5 km s^{-1}.

Key words: galaxies: individual: NGC 1614 – galaxies: starburst – methods: data analysis

1 INTRODUCTION

Numerical simulations have shown that collisions between gas-rich galaxies are efficient at transporting large quantities of molecular gas into the galactic nuclei (Barnes & Hernquist 1996). A strong burst in the star formation rate (called as a starburst) may occur in such cases, due to the concentration of gas, and an active galactic nucleus (AGN) may be activated. This has been observed in many luminous and ultra-luminous infrared galaxies (LIRGs and ULIRGs, respectively). However, mid-infrared spectroscopic studies (e.g. Lutz et al. 1998) suggest that most of these objects are powered by star formation. Hence, LIRGs and ULIRGs can be used for studying the star formation process on extreme scales.

NGC 1614 is a nearby LIRG situated at a distance of 67.8 Mpc (Crook et al. 2007) and having a high infrared luminosity of $L_{IR} = 10^{11.65} L_{\odot}$ (Armus et al. 2009). In optical wavelengths, this galaxy has two fairly symmetric spiral arms around a bright center (Neff et al. 1990). Several tracers such as Paschen-α (Alonso-Herrero et al. 2001), radio continuum (Olsson et al. 2010) and CO (2–1) (König et al. 2013) show a circumnuclear ring in the galaxy. Neff et al. (1990) observed the outer structure of NGC 1614 to contain plumes or tidal tails which can be attributed to an earlier merger or an interaction with another galaxy. Using numerical simulations, Väisänen et al. (2012) suggested that it is a minor merger with mass ratio of 1:3 – 1:5. NGC 1614 has been visually classified as a merger remnant by Rothberg & Joseph (2004) due to the lack of a nearby companion. It has also been deemed consistent with signatures of a starburst dominated galaxy lacking a strong AGN as per HCN (4–3) and HCO$^+$ (4–3) observations (Costagliola et al. 2011; Imanishi & Nakanishi 2013).

The archival dataset used in this paper is summarized in Section 2. Data calibration steps and the imaging steps are explained in Section 3 and Section 4, respectively. The analysis of the final images has been outlined in Section 5. A final summary of the work is given in Section 6. The optical convention for velocities, $v = cz$, has been used throughout the paper. A Hubble constant of $H_0 = 75\,\mathrm{km\,s^{-1}\,Mpc^{-1}}$ was used.

2 OBSERVATIONAL DATA

The *Common Astronomy Software Applications*[1] (CASA; McMullin et al. 2007) package was used for visualizing, calibrating and imaging the data. CASA is a collection of applications with a number of tasks and tools used for reduction and analysis of radio astronomical data.

The dataset was first imported into CASA visibility file format, known as a Measurement Set (MS), from the ALMA Science Data Model (ASDM) format using the task `importasdm`. The summary of the MS was generated using `listobs` and the antenna distribution was plotted using `plotants`.

The CO (1–0) observations took place on the 30^{th} of August, 2014 using 35 12 m ALMA antennas with Band 3 receivers. These 35 antennas give us a total of 595 baselines. From Figure 1, we see that the minimum separation between two antennas is about 33 m (PM03 and DA61) and the maximum baseline is about 1060 m (DV25 and DV62). A strong quasar, J0423-0120 was used as a bandpass and phase calibrator. The same quasar was for calibrating the flux. 25 unique Spectral Windows (SpWs) were used for all the observations. The Water Vapour Radiometer (WVR) measurements were stored in SpW 0. The science data was

* E-mail: ziad@uni-bonn.de

[1] Release version 4.6.0 (https://casa.nrao.edu/)

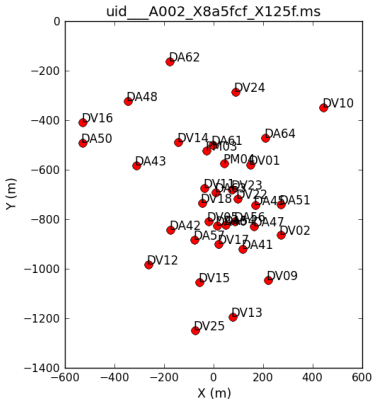

Figure 1. The antenna distribution of our dataset, generated using the CASA task `plotants`.

stored in SpW 17, 19, 21 and 23. These SpWs had a 1920 spectral channels each with a channel width of 976.5 kHz. The SpWs had a bandwidth of 1.875 GHz resulting in a velocity resolution of $v_{res} = 2.5\,\mathrm{km\,s^{-1}}$. The remaining SpWs were used for bandpass, phase, flux, pointing, atmosphere and sideband ratio calibration.

3 DATA CALIBRATION

Interferometers measure the complex visibilities of the source. The goal of calibration is to correct the observed visibilities, $V'_{ij}(\nu, t)$, so that we can get as close as possible to the true visibilities, $V_{ij}(\nu, t)$. The true visibilities are affected by different time and frequency dependent gains as per Equation 1,

$$V'_{ij}(\nu, t) = V_{ij}(\nu, t) \times G_{ij}(\nu) \times B_{ij}(t) \quad (1)$$

where, ν is the frequency, t is the time, $G_{ij}(\nu)$ is the complex frequency dependent gain and $B_{ij}(t)$ is the complex time dependent gain of the ij-th baseline.

3.1 *A Priori* Calibration

A priori calibrations are done using the information provided with the dataset. All the autocorrelation data was flagged first using the CASA task `flagdata`. Then, the data from intents like pointing, atmosphere and sideband ratio was flagged. The data affected by antenna shadowing, especially in compact configurations, was also flagged.

The T_{sys} measurements from the dataset were used to create a calibration table using `gencal`. Similarly, a WVR calibration table was generated using the task `wvrgcal`. These calibration tables were then applied to the fields in our observations using the task `applycal`. The T_{sys} and WVR calibration tables are used to generate second order corrections to $G_{ij}(\nu)$ and $B_{ij}(t)$, respectively.

On inspecting the T_{sys} calibration tables, it was seen that two antennas, DA50 and DA41, were behaving in an unexpected manner. Hence, all the data from those two antennas was flagged. The diagnostic plots showing the unexpected behavior of DA50 and DA41 are shown in the appendix Figures A1 and A2 on page 7, respectively.

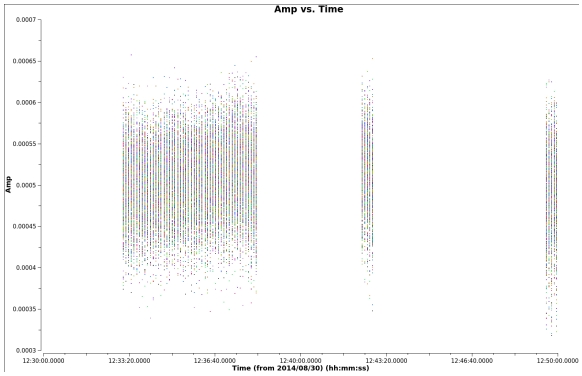

Figure 2. Amplitude vs. Time plot of the uncorrected data

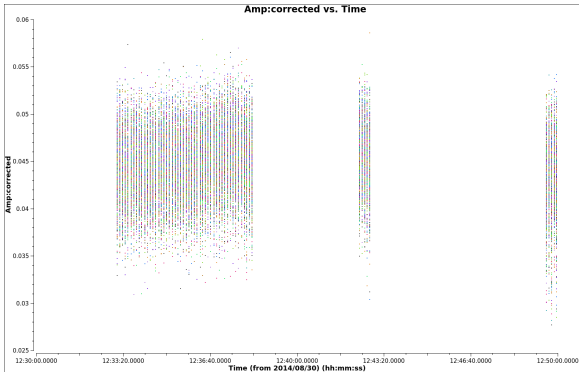

Figure 3. Amplitude vs. Time plot of the corrected data

After the *a priori* calibration was applied, the results of the calibration were checked by plotting the amplitude with respect to time of the calibrator, J0423-0120, while averaging all the channels together. The plots, generated using the for the uncorrected and the calibrated data are shown in Figure 2 and 3, respectively. We see that the scale of the amplitude has changed after the calibration.

As mentioned in Section 2, the science target data was stored in SpWs 17, 19, 21 and 23. The data from these SpWs was split out into a new MS using the task `split` and a summary of this new MS was generated using `listobs`. All the following calibrations were applied to this new MS.

The plots shown in Figures 4a and 4b on page 3 were plotted from the data in the new MS.

3.2 Bandpass Calibration

Bandpass calibration corrects the frequency-dependent complex gain, $G_{ij}(\nu)$ in Equation 1, by using a bandpass calibrator. A good bandpass calibrator is a bright source with a spectrum lacking a lot of features. It may or may not be near the science target. In this step, estimates of the amplitude and phase errors, over the bandpass, to get a correct spectral representation of the sky are done.

Before combining all the scans together and doing the bandpass calibration, global phase variations with time, which are independent of frequency, need to be corrected for. This is done by using the CASA task `gaincal` to estimate

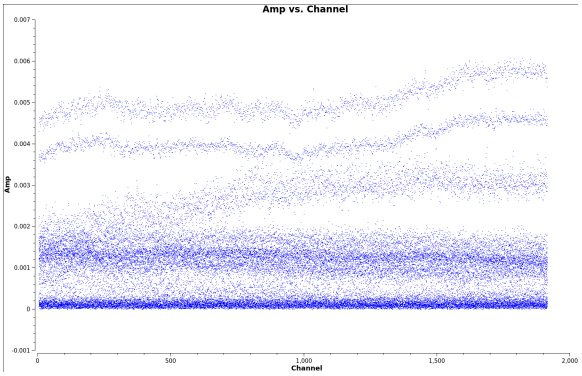

(a) Amplitude vs. Channel plot of the science SpWs while averaging all the baselines and averaging the time over each scan

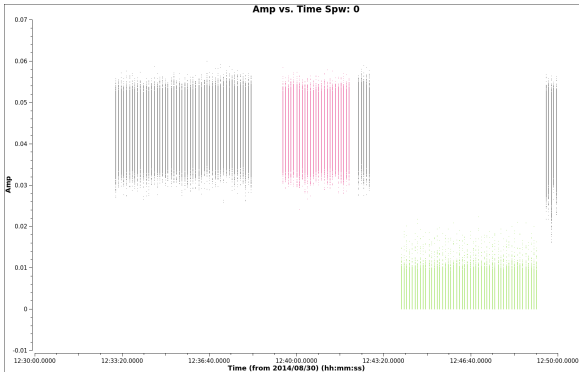

(b) Amplitude vs. Time plot with different colors representing different fields of observation while averaging all channels

Figure 4. Amplitude change with Frequency (Channel) and Time plots

(a) Uncalibrated Data

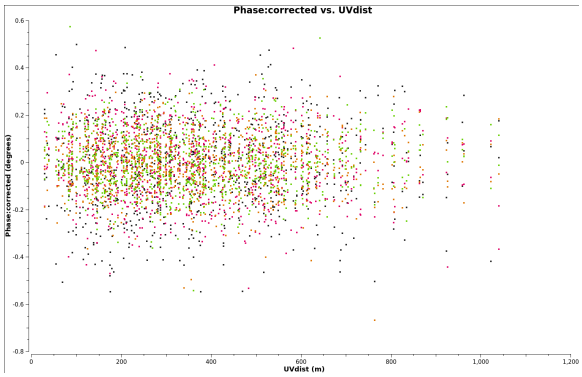

(b) Calibrated Data

Figure 5. Phase vs. UV Distance plots with channel and integration averaging

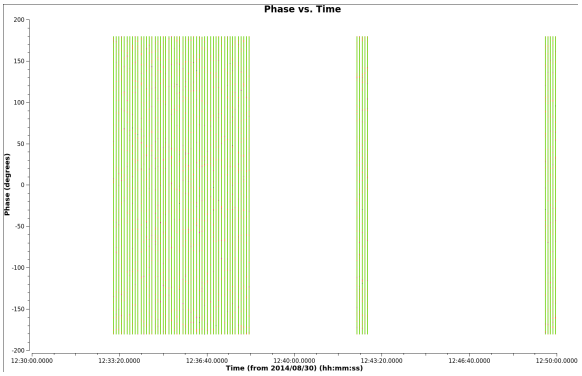

(a) Uncalibrated Data

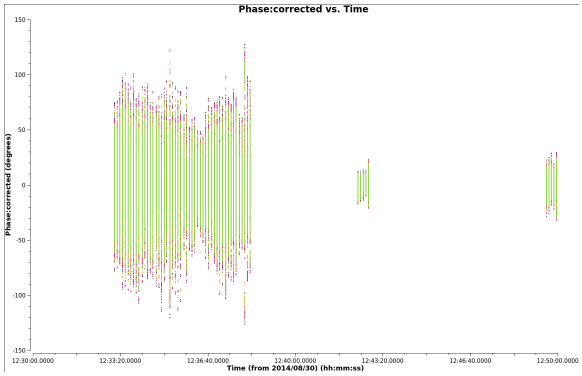

(b) Calibrated Data

Figure 6. Phase vs. Time plots with just the channel averaging

the corrections in phase for each integration. The calibration table generated at this step is shown in Figure A3 on page 8.

The bandpass corrections were generated using the task `bandpass` while applying the previously generated phase corrections on-the-fly. The bandpass calibration table was inspected using the plots shown in Figures A4 and A5 on page 9 and page 10, respectively.

3.3 Flux and Phase Calibration

Flux and Phase calibrations are done to determine the time-dependent complex gain, $B_{ij}(t)$ from Equation 1. To get absolute flux value measurements, we need a good flux calibrator. It is an object with known flux e.g. 3C286 and 3C48. Phase calibration is required to achieve a high signal to noise ratio and to get a correct representation of the sky. Phase calibrator must be a bright point source near the science target.

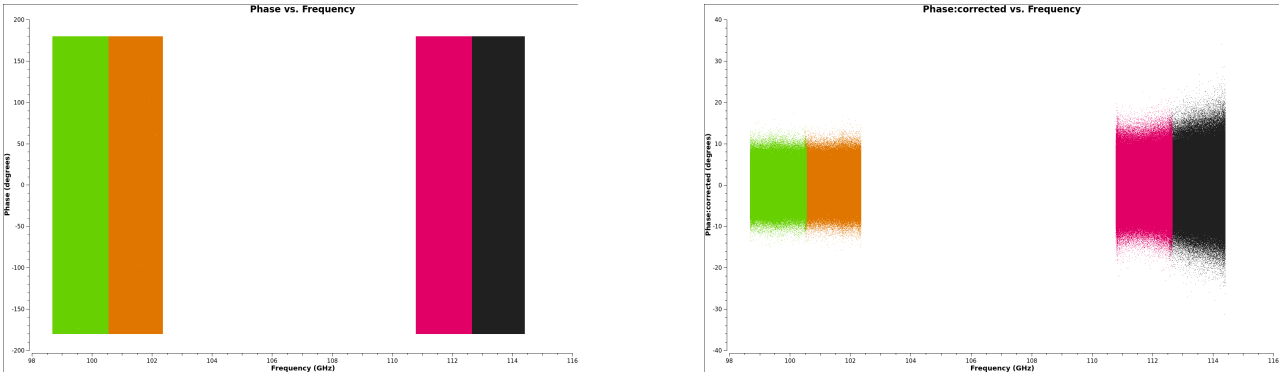

(a) Uncalibrated Data (b) Calibrated Data

Figure 7. Phase vs. Frequency plots with time averaging

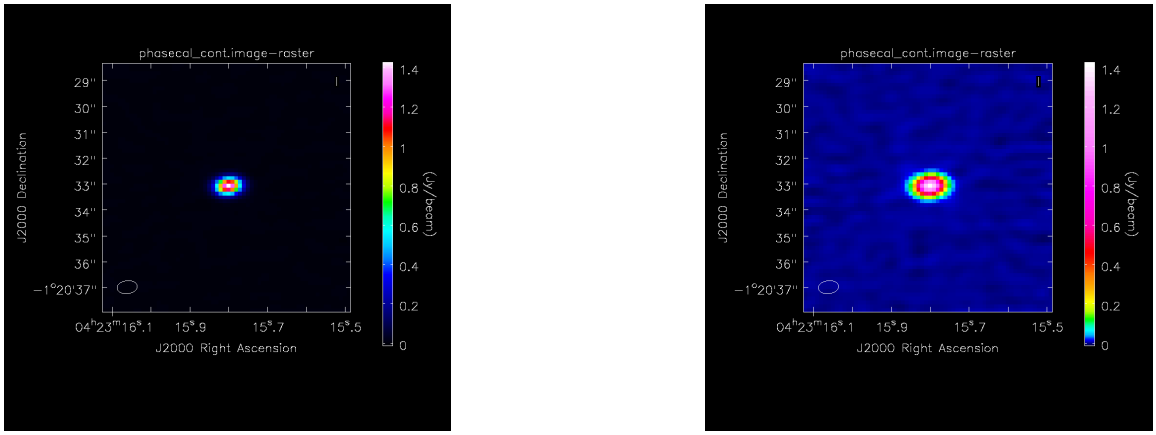

(a) Linear Scale (b) Logarithmic Scale

Figure 8. J0423-0120, the phase calibrator

Using the task `setjy`, a model of the flux calibrator was set. The ALMA Science Portal's Calibrator Catalogue (https://almascience.nrao.edu/sc/) was used for this purpose. Before inferring the actual amplitude calibration table, the global phase variation table with the bandpass calibration table applied on-the-fly was measured for each integration using `gaincal`. The amplitude corrections were then measured, again using `gaincal`, while applying the bandpass and global phase corrections on-the-fly.

Until now, all the calibrators, except the flux calibrator, had unknown fluxes. Hence, the flux scales from our flux calibrator were transferred to other calibrators using the task `fluxscale`. Then the phase calibration table was inferred for each scan while applying the bandpass table on-the-fly.

Since all the calibration tables are inferred, they were applied to all the observed fields using the task `applycal`. The plots in Figures 5, 6 and 7 were used to inspect the calibrated data. The plots for the calibrated data, ideally, are supposed to be flat with a phase of 0°. The plots for the calibrated data were not flat and had some phase variations.

4 IMAGING

In this section the CLEAN algorithm (Högbom 1974) was used extensively. CLEANing is done in CASA by using the task `clean`.

4.1 Imaging the Phase Calibrator

As mentioned in Section 3.3, a phase calibrator should be a point source. A check on the calibration can be performed by imaging the phase calibrator. If it is seen to be a point source image without any artifacts, it can be concluded that the calibrations have worked.

To image the phase calibrator, the CLEAN algorithm was used on the MS with by selecting the phase calibrator field and creating a mask around it. The CLEAN threshold was selected to be 0.75 mJy. An image of 256×256 pixels was generated. The pixel size should be around 3 to 5 times smaller than the Full Width at Half Maximum (FWHM) of the synthesized beam. The FWHM of the synthesized beam, for ALMA Band 3 and a maximum baseline of 0.65". Hence, the pixel size was selected to be 0.15". The images of the phase calibrator with linear and logarithmic scales are shown in Figures 8a and 8b, respectively.

The SpWs with the scientific target data were split out into a new MS. This was done using the task `split` and

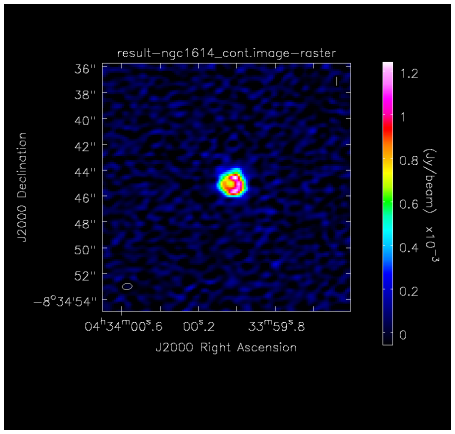

(a) Robust 0.0 with a beam size of 0.75”×0.48” and RMS noise level of 0.057 mJy/beam

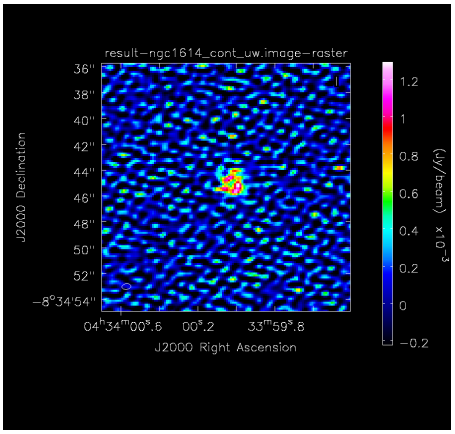

(b) Robust -2.0 with a beam size of 0.70”×0.45” and RMS noise level of 0.223 mJy/beam

Figure 9. Continuum Maps

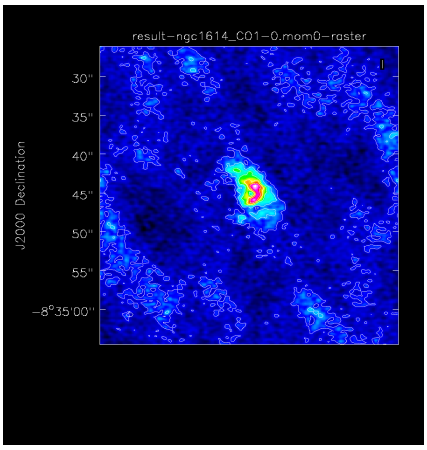

(a) Moment-0 map with contours at 3σ, 6σ, 9σ and 12σ and showing the integrated flux

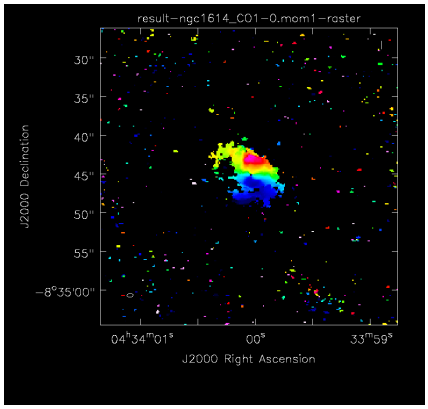

(b) Moment-1 map showing the velocity field

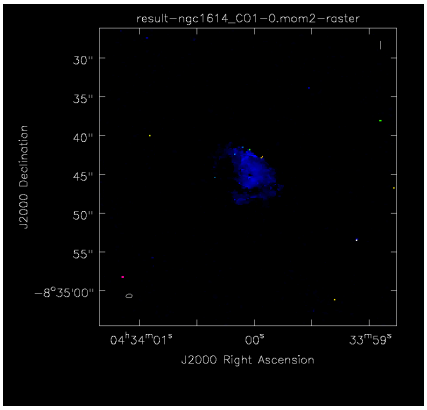

(c) Moment-2 map showing the velocity dispersion

Figure 10. Moment Maps generated by collapsing the line emission data cube

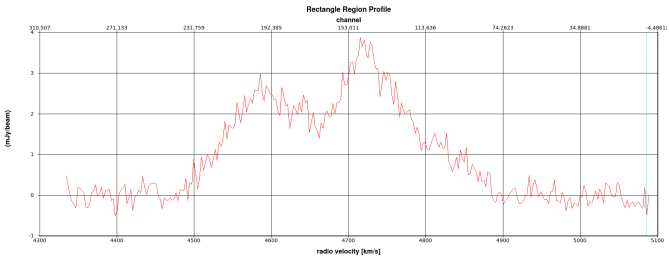

(a) Spectrum of the line emission, extracted from the data cube with the signature two-horned peak of a galaxy

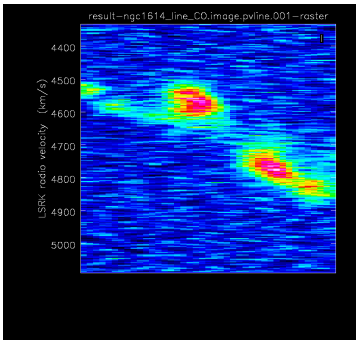

(b) P-V Diagram, generated using the PV Tool in CASA and the Moment-1 map

Figure 11.

selecting the field of NGC 1614. The plots of Amplitude change with Frequency (see Figure A6 on page 11) were used to determine which channels contained continuum data and which ones contained line emission data.

4.2 Continuum & Line Imaging

Visually inspecting Figure A6 shows that except channels 800 to 1100 of SpW 0, all the remaining channels contain continuum emission data. Hence, these channels were selected in CLEAN to create a dirty map of the continuum. A dirty map is created by using the CLEAN algorithm without any threshold and running it just once. The RMS noise of an area in the dirty map without any emission features was used as the threshold for creating a CLEAN continuum map. This noise was estimated using the task `imstat`. Two CLEAN continuum maps were created, one with a Robust parameter of 0.0 and other with a Robust parameter of -2.0. The Robust parameter decides how much weight is to be given to different baseline scales. A smaller number gives a higher weight to longer baselines, thus improving resolution. Whereas, a higher number gives a higher weight to smaller baselines. Both the continuum maps are shown in Figures 9a and 9b. As expected, the restoring beam size is smaller, meaning higher resolution, and the RMS noise level is higher for Robust -2.0 image.

Before imaging the line emission, a linear (order 1) baseline was fitted and subtracted from the data in the UV plane using the CASA task `uvcontsub`.

For imaging the line emission, a similar procedure to continuum imaging was followed. The difference here is that instead of creating a single map, a data cube is created. This data cube has two position axes and a third velocity (Kinematic Local Standard of Rest) axis. It had a velocity resolution of 2.5 km s^{-1}. The CLEAN data cube thus generated had a restoring beam size of 0.81"×0.50" and an RMS noise level of 5.363 mJy/beam.

5 IMAGE ANALYSIS

On collapsing the the data cube along the into moments, the moment maps are generated. The zeroth moment map, Figure 10a, is generated by summing up the data cube along the velocity axis. The total integrated flux was calculated by selecting the region over which the galactic emission is seen. By using the task `imstat` on this region, the total integrated flux was found to be 144.5 Jy km s^{-1}.

The first moment map, Figure 10b, is generated by integrating the product of velocity and intensity over the velocity axis. The P-V diagram, shown in Figure 11b, is generated by selecting a slit along the velocity gradient seen in the moment-1 map.

And, the second moment map, shown in Figure 10c, gives us the integration of the product of velocity and squared intensity over all velocities.

6 SUMMARY

The data set of ALMA Band 3 observations of an LIRG, NGC 1614, was calibrated using CASA. J0423-0120, a strong quasar, was used as the bandpass, flux and phase calibrator. During the *a priori* calibration, it was found that two antennas, DA41 and DA50, out of the total 35 behaved unexpectedly and, hence, were flagged. The data was then calibrated for bandpass, flux and phase. The RMS noise of the continuum map was found to be 0.057 mJy/beam with a restoring beam size of 0.75"×0.48" (Robust 0.0). The line emission data cube had an RMS noise level of 5.365 mJy/beam with a restoring beam of 0.81"×0.50". The total integrated flux of the galaxy was found to be 144.5 Jy km s^{-1}. The spectrum of line emission and the P-V diagram were generated.

ACKNOWLEDGEMENTS

The use of CASA Release 4.6.0 (https://casa.nrao.edu) is acknowledged. ZM would like to thank B. Magnelli, S. Mühle and other members of the German ALMA ARC Node for the conducting the course on Radio Interferometry. ZM would also like to thank Jackie Ma Yik Ki for his guidance throughout this work.

REFERENCES

Alonso-Herrero, A., Engelbracht, C. W., Rieke, M. J., Rieke, G. H., & Quillen, A. C. 2001, ApJ, 546, 952
Armus, L., Mazzarella, J. M., Evans, A. S., et al. 2009, PASP, 121, 559
Barnes, J. E., & Hernquist, L. 1996, ApJ, 471, 115
Costagliola, F., Aalto, S., Rodriguez, M. I., et al. 2011, A&A, 528, A30
Crook, A. C., Huchra, J. P., Martimbeau, N., et al. 2007, ApJ, 655, 790
Högbom, J. A. 1974, A&AS, 15, 417
Imanishi, M., & Nakanishi, K. 2013, AJ, 146, 47
König, S., Aalto, S., Muller, S., Beswick, R. J., & Gallagher, J. S. 2013, A&A, 553, A72
Lutz, D., Spoon, H. W. W., Rigopoulou, D., Moorwood, A. F. M., & Genzel, R. 1998, ApJ, 505, L103
McMullin, J. P., Waters, B., Schiebel, D., Young, W., & Golap, K. 2007, Astronomical Data Analysis Software and Systems XVI, 376, 127
Neff, S. G., Hutchings, J. B., Standord, S. A., & Unger, S. W. 1990, AJ, 99, 1088
Rothberg, B., & Joseph, R. D. 2004, AJ, 128, 2098
Olsson, E., Aalto, S., Thomasson, M., & Beswick, R. 2010, A&A, 513, A11
Väisänen, P., Rajpaul, V., Zijlstra, A. A., Reunanen, J., & Kotilainen, J. 2012, MNRAS, 420, 2209

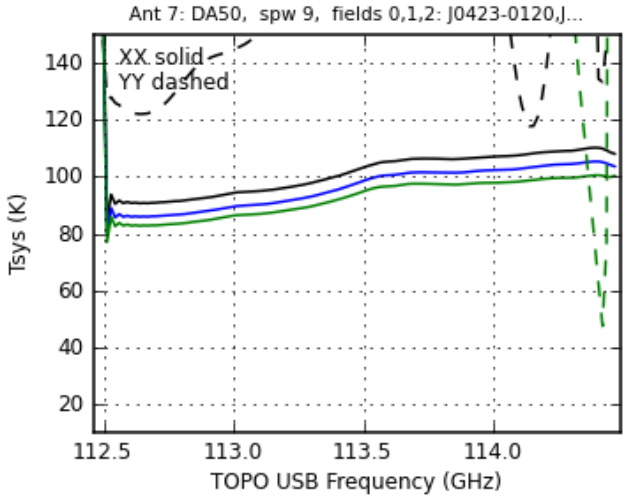

Figure A1. T_{sys} calibration table plot for DA50 showing unexpected behavior of the YY correlation data

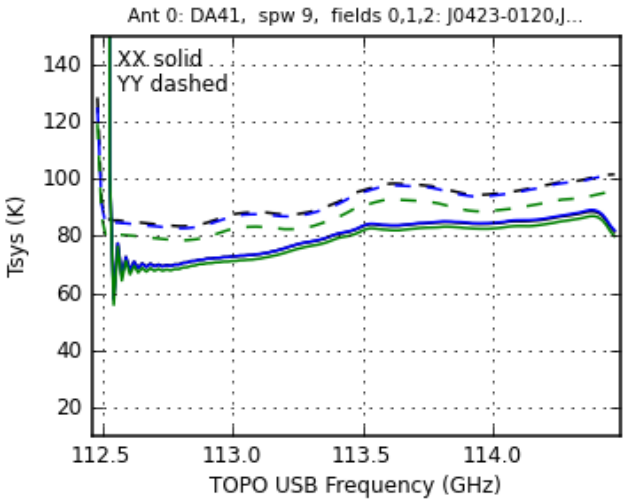

Figure A2. T_{sys} calibration table plot for DA41 showing spurious oscillatory behavior

APPENDIX A: ANCILLARY PLOTS

This paper has been typeset from a TEX/LATEX file prepared by the author.

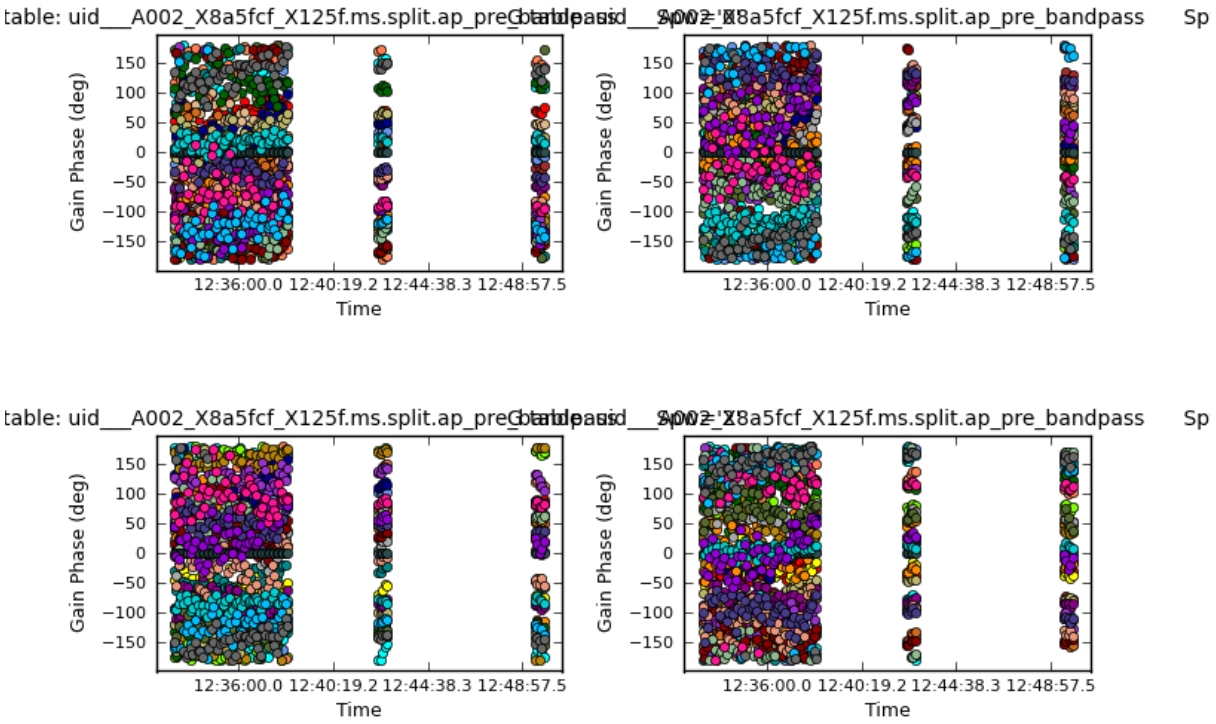

Figure A3. The pre-bandpass global phase variation calibration table plots

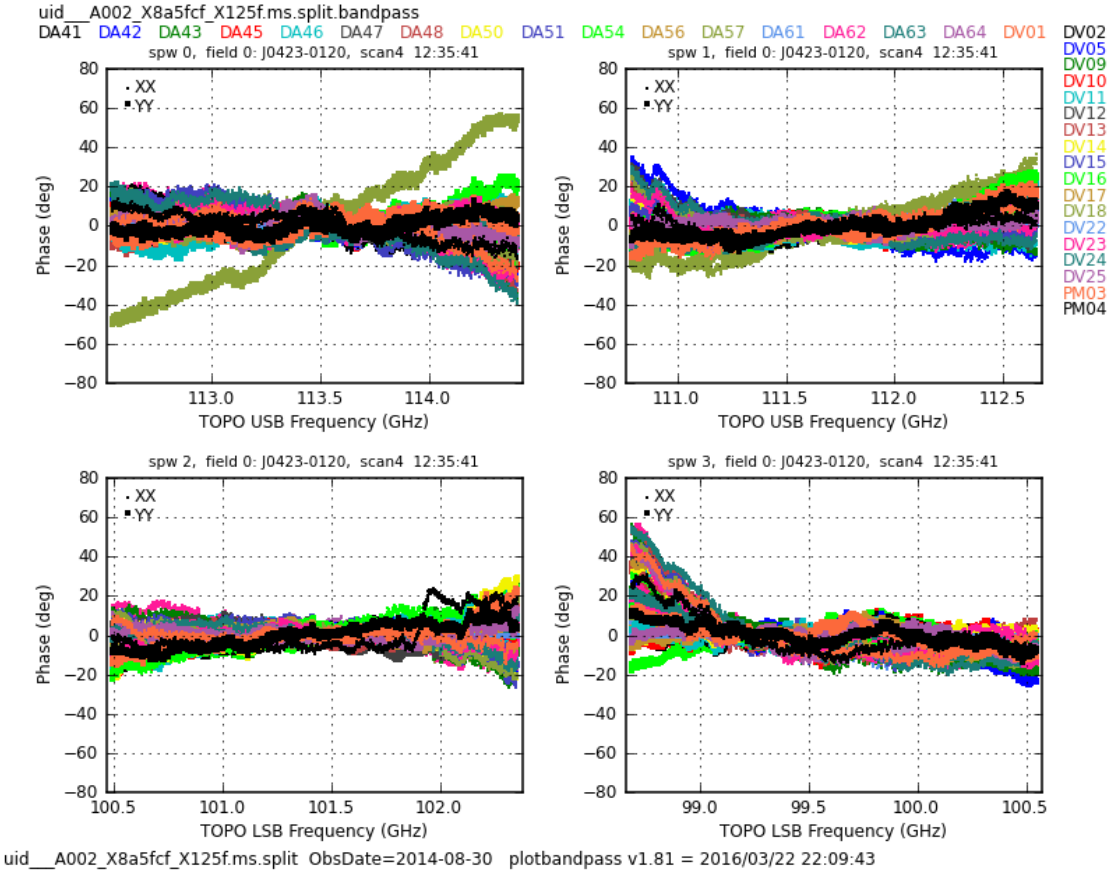

Figure A4. Phase vs. Frequency plot of the bandpass calibration table

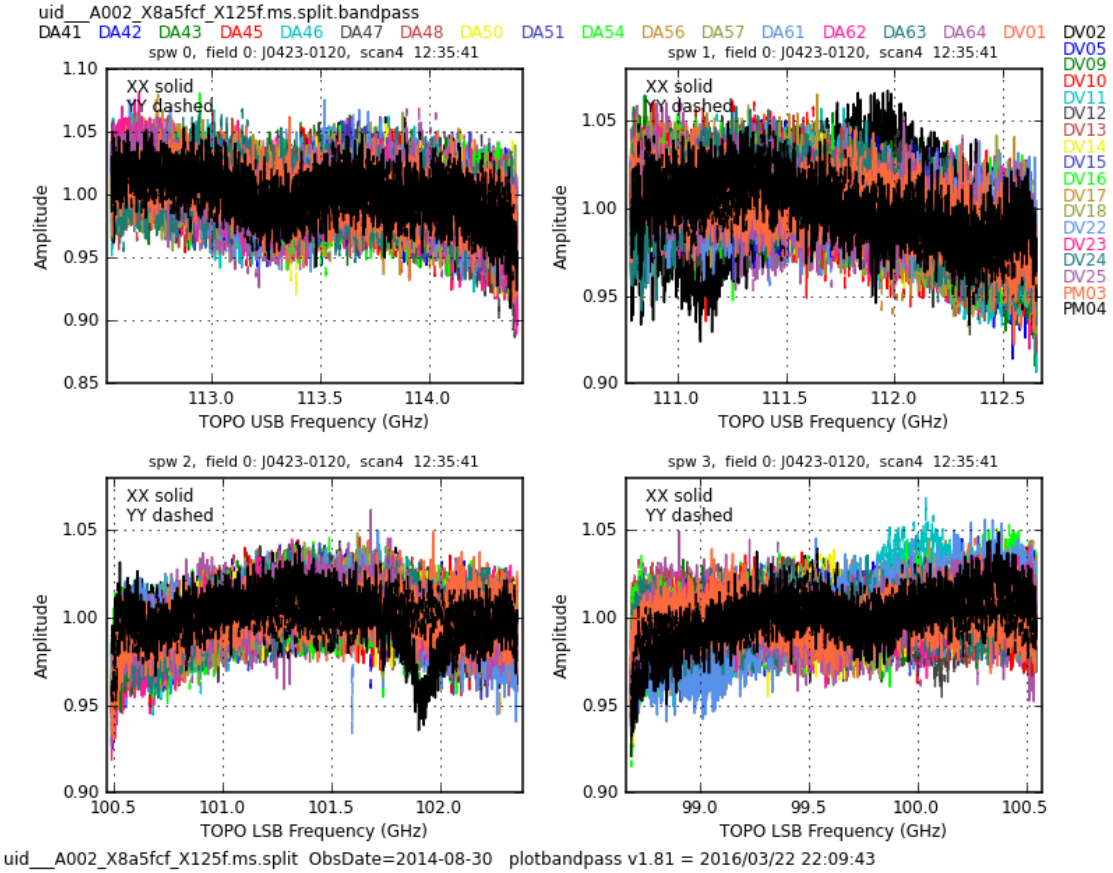

Figure A5. Amplitude vs. Frequency plot of the bandpass calibration table

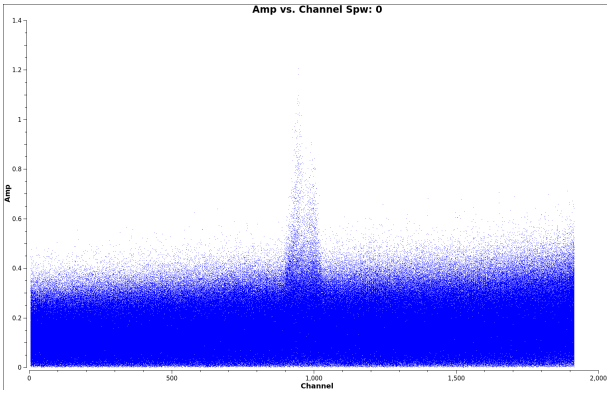

(a) SpW 0

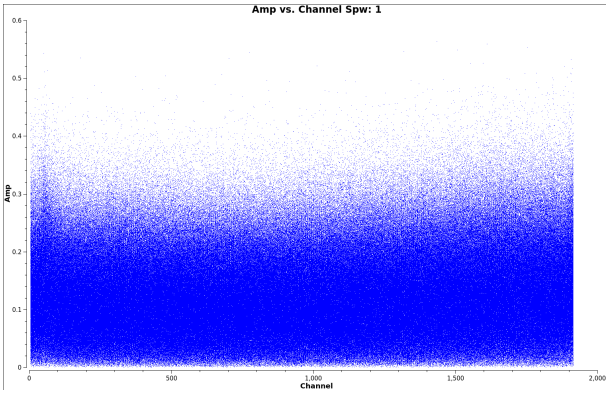

(b) SpW 1

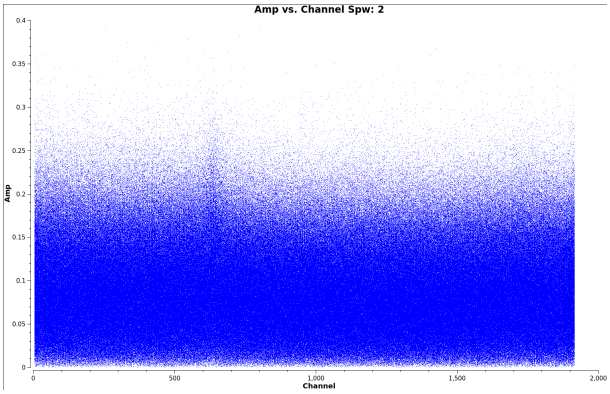

(c) SpW 2

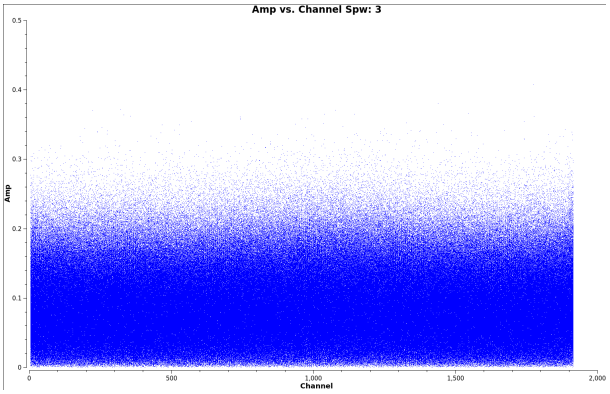

(d) SpW 3

Figure A6. The Amplitude vs. Channel plots of the final science SpWs.